18.2 IMPACT OF THE VARIATIONS OF PRECIPITATION PARTICLE PARAMETERS WITHIN THE SAME MICROPHYSICS SCHEME IN RADAR DATA ASSIMILATION USING EnKF DATA ASSIMILATION TECHNIQUE

Nusrat Yussouf[1] and David J. Stensrud[2]
[1]Cooperative Institute for Mesoscale Meteorological Studies, Norman, Oklahoma
[2]NOAA/National Severe Storms Laboratory, Norman, Oklahoma

1. INTRODUCTION*

The radial-velocity and reflectivity observations of severe weather events like thunderstorms and tornadoes from WSR-88Ds can provide important information for the initialization of numerical storm-scale prediction models using the Ensemble Kalman Filter (EnKF) approach (Snyder and Zhang 2003, Zhang et al. 2004, Dowell et al. 2004a, Xue et al. 2006, Aksoy et al. 2009). Research reveals that approximately a 30-60 minutes assimilation window is sufficient to initialize a severe storm into the model using WSR-88D 5-6 minute volume scan data. However, while the WSR-88D data assimilation in storm-scale model provide a good quality analyses, reliable short-term forecasts from these good quality analyses still remains a challenge to the researchers in the data assimilation community.

One of the major sources of error in storm-scale data assimilation and forecasts is the microphysical scheme used to represent the microphysical characteristics of the storms in the model. The development of a microphysics scheme is based on 1) a number of different phase changes of water species and 2) a number of different interactions between cloud and precipitation particles. Thus, many assumptions are needed to make these schemes both realistic and computationally affordable (Stensrud 2007). The most commonly used type of microphysical scheme in storm-scale modeling is a single-moment bulk microphysics scheme that predicts only the particle mixing ratios of the hydrometeors. However, the precipitation particles that are represented in the various single-moment bulk microphysics schemes tend to differ from one another.

A single-moment scheme uses a specified functional form with constant values of intercept parameters and densities of hydrometeors for the calculation of hydrometeors size distributions (Stensrud 2007) that are defined somewhat arbitrarily and remain constant throughout the simulation. However, several observational studies indicate that the particle densities and intercept parameters of hydrometeor distributions can vary widely within a single storm and among storms (Gunn and Marshall 1958; Houze et al. 1979, 1980; Mitchell 1988; Pruppacher and Klett 2000; Cifelli et al. 2000; Brandes et al. 2007). Moreover, Gilmore et al. (2004) show that reasonable selections of intercept parameters and density of hail/graupel yield substantial and operationally important differences in simulations of thunderstorms in terms of storm structure, severity and intensity. Snook and Xue (2008) find that varying the intercept and density parameters within their typical uncertainty range yield a wide range of solutions from the same set of initial and environment conditions. Thus applying predefined constant parameters for precipitation particles cannot adequately represent the particle microphysical characteristics and can lead to significant errors in the analyses and forecasts of severe storms.

Determining the suitable values for the microphysical parameters in storm scale data assimilation however is very difficult due to the lack of in situ cloud observations. Since the selection of microphysical parameters in storm-scale modeling has profound impact on the analyses and forecasts of severe weather events, and an arbitrary selection of those parameters may lead to significant error, one approach to account for the uncertainty in the storm-scale EnKF system is to vary the microphysical parameters within the same microphysics scheme. Results from Fujita et

* *Corresponding author address:* Nusrat Yussouf, Cooperative Institute for Mesoscale Meteorological Studies, 120 David L. Boren Blvd. Norman, OK, 73072;
e-mail: nusrat.yussouf@noaa.gov

al. (2007) and Stensrud et al. (2009) indicate that an ensemble with multiple physical parameterizations and initial condition perturbations yields better analyses and forecasts than an ensemble with only initial condition or physics perturbations. Therefore in an effort to explore the impact of variations in parameters within the same microphysics scheme in storm scale system, Observing System Simulation Experiments (OSSEs; Lord et al. 1997) are conducted using a range of different realizations of the intercept and density parameters using an EnKF data assimilation technique. The simulation of a supercell storm is conducted using two different microphysics schemes. Radial-velocity and reflectivity observations are then constructed from the reference solutions and are assimilated using the ensemble Kalman filtering technique on the same numerical model that produced the reference simulation. The first set of experiments is based on assumptions of a perfect model in which both the truth simulation and the ensemble system use the same microphysics scheme. The second set of experiments is based on imperfect model assumptions in which the microphysics scheme for the truth simulation and the microphysics scheme for the assimilation system are different. The imperfect model assumption includes error in the forecast models, particularly from the microphysical parameterization. The storm-scale model, simulated radar dataset and the experimental design are described in section 2. Section 3 presents the results obtained from the EnKF analysis and forecasts, followed by a final discussion in section 4.

2. ASSIMILATION SYSTEM AND EXPERIMENTAL DESIGN

The Collaborative Model for Multiscale Atmospheric Simulation (COMMAS; Wicker and Skamarock 2002; Coniglio et al. 2006) model used in this study is a nonhydrostatic compressible numerical cloud model. The data assimilation scheme used is based on the ensemble square-root filter (EnSRF) of Whitaker and Hamil (2002). The reflectivity and radial velocity observations are assimilated in the filter serially. Each time an observation is assimilated, the ensemble mean and each of the ensemble members are updated for each model variable at each grid point within 4 km of the observation. Details of the EnSRF system used in this study can be found in Dowell et al. (2004a). In this study, a 40 member ensemble is used, and the number of observations assimilated during each 1-min assimilation period ranges from 630 to 25360, depending on the location of the radar relative to the supercell, height of radar scans and supercell intensity.

This study uses a radar emulator that generates radial-velocity and reflectivity observations from the reference simulations in native radar coordinates using a simplified version of a realistic volume averaging technique (Wood et al. 2009). The *Z*, *u*, *v* and *w* wind components at model grid points within the beamwidth are scanned with the radar emulator to produce the WSR-88D radar reflectivity and radial velocity observations. Details of the radar emulator are discussed in the Yussouf and Stensrud (2009). To reduce the heavy computational burden of observation assimilation, the reflectivity and radial velocity observations used in this study are created along each radial at a coarser 1.0-km range sampling interval instead of the 0.25 km interval available from the radars. The antenna half-power beamwidths are assumed to be 0.89^{o} for this study with 1.0^{o} azimuth interval and a 1.39^{o} effective beamwidth. The synthetic radar observations are generated using Volume Coverage Pattern (VCP) 11 precipitation mode scanning strategy consisting of 14 elevation angles. To assimilate the WSR-88D radar observations more realistically, the WSR-88D observations are generated for 2-3 sweeps every minute rather than assuming the entire volume is collected simultaneously. Out of the 14 sweeps, the lower 12 sweeps of observations are generated 3 sweeps per minute for the first 4 min with the remaining upper 2 sweeps valid for the fifth minute of the volume scan. To account for the measurement and sampling errors for radial velocity and reflectivity observations, random numbers are drawn from a Gaussian distribution of zero mean and standard deviations of 2 m s^{-1} and 2 dBZ, respectively, and are added to the observations. Moreover, the radar is stationary while the model domain moves with the simulated storm; all experiments in this study are conducted using a single radar to observe the supercell storm.

2.1. *The two truth simulations and synthetic radar observations*

Two simulation runs of a supercell thunderstorm are conducted using the classic Weisman-Klemp analytic sounding (Weisman and Klemp, 1982) with a quarter circle hodograph for the vertical wind shear profile. The model domains for the truth runs are 100 km wide with 1-km resolution in the horizontal and 18 km tall in the vertical direction. The domains are vertically stretched from 100 m vertical spacing at the bottom to 700 m vertical spacing at the domain top. The 2 h long simulations are initiated with an ellipsoidal thermal bubble of 2.5 K with 10 km radius in the horizontal direction and 1.4 km radius in the vertical direction that is placed at the center of the domain at t = 0 min. The ellipsoidal thermal bubble develops into a convective cell within the first 30 mins of the simulations and the first echoes are seen by the radar emulator at around t = *25* min. Over the next 30 min, the convective cell splits into two cells, one moving right towards the east and the other moving towards the northeast. During the second hour of the simulations, the right-moving cell tends to dominate the system with a few short lived smaller cells developing in between the two main cells. The domain grids are translated at u = 17 and v = 7 m s^{-1} to keep the main storm near the center of the model domains.

The first truth simulation applies the Gilmore et al. (2004) version of the Lin-Farley-Orville (Lin et al. 1983) single-moment bulk microphysics scheme (Truth_LFO hereafter). The LFO scheme contains three ice categories (i.e. ice crystals, snow and hail/graupel) and calculates the mixing ratios of six water species: water vapor, cloud water, cloud ice, rain, snow and hail/graupel. The second truth simulation applies the 10-ICE (Straka and Mansell, 2005) single-moment bulk microphysics scheme (Truth_10ICE hereafter) to represent more realistic storm characteristics. It has the same two water particle categories (cloud water and rain) as the LFO scheme and ten ice categories (i.e. 6 graupel and hail categories, 3 ice categories and snow) that are characterized by habit, size and density. The extra ice hydrometeor categories that are included in the 10ICE scheme better represent the range of precipitation ice characteristics in a storm system. It also improves the treatment of conversion from one ice categories to another with the changes in habit, density and terminal velocity (Straka and Mansell, 2005). Both microphysics schemes assumes a monodisperse particle size distribution for cloud water and cloud ice and approximate an inverse exponential form (Marshall and Palmer 1948) for the particle size distributions of rain and ice categories as follows:

$$n_x(D) = n_{0x} e^{-\lambda_x D_x} \qquad (1)$$

where x is rain or ice categories, D is the particle diameter (m), n is the number of particles per unit volume (m^{-4}), λ is the slope parameter that defines the decrease in particle counts as diameter increases (m^{-1}) and n_{0x} is the intercept parameter that defines the maximum number of particles per unit volume at $D = 0$ size. The slope parameter varies with mixing ratio and is given by

$$\lambda_x = \left(\frac{\pi \rho_x n_{0x}}{\rho q_x} \right) \qquad (2)$$

where ρ_x is the density of the particle, ρ is the air density, and q_x is the mixing ratio. From equation (1) and (2), it is obvious that the particle size distribution is a function of n_{0x} and ρ_x. The values of the density and the intercept parameters used for the truth simulation from the two microphysics scheme are given in Table 1.

The truth runs from the two microphysics schemes produce a similar supercell storms, however there are differences in the location, strength and structure of the storm as shown in Fig. 1. The cold pool at the lowest model level from Truth_10ICE (Fig. 1b) is colder than the cold pool from Truth_LFO (Fig. 1a) after 35 mins of the simulation. The high-reflectivity core of the southern cell from the Truth_LFO is more intense than the reflectivity core of the southern cell from Truth_10ICE and the mid-level vertical vorticity also differ from each other (Fig. 1 e and f). Similar differences also are found for other variables at other vertical levels of the model domain at other simulation times.

2.2. The ensemble configuration and OSSE design

Each member of the 40 member ensemble uses the same classic Weisman-Klemp sounding with quarter circle hodograph in a horizontally homogeneous environment to define the initial environmental condition. The domain size and grid resolution for the ensemble members are identical to the truth runs. To facilitate the development of storms, 3 thermal bubbles (i.e. 1.5 K maximum ellipsoidal θ perturbations) with 7.5 km radius in the horizontal direction and 2.0 km radius in the vertical direction at random locations within the 40 km to 60 km portion of the domain in x and y directions and within 0.25 to 2.25 km in z direction are introduced at the initialization time ($t = 0$) to each ensemble member following Synder and Zhang (2003) and Dowell et al. (2004a, b). This method of initialization is very helpful as the thermal bubbles initiate convective cells and produce the covariance information needed for the ensemble to successfully assimilate the radar data. The domain of the ensemble also moves at $u = 17$ and $v = 7\ m\ s^{-1}$ following the truth run to keep the storm inside the domain.

After initializing the ensemble members at $t = 0$, the members are integrated forward in time for 25 min before the assimilation of first observations. During this period, the θ perturbations within the center 20 km x 20 km area of the domain initiate convective cells in the ensemble members (Synder and Zhang 2003; Dowell et al. 2004a, b; Aksoy et al. 2009). The 30 min long assimilation period starts at t = 25 min and ends at t = 54 min. During this assimilation period, 6 volume scans of WSR-88D observations are assimilated. The radar is located at x = -3.6 km and y = -4.9 km from the southwest corner of the domain during the first volume scan. The observations valid within 1 min of the current time are assimilated followed by advancing the ensemble members 1 min to the next observation time. No covariance inflation or thermal perturbations are added to the members to maintain the ensemble spread during the assimilation cycles. After 30 min of data assimilation, the ensemble members are used to produce a 1-h forecast. Moreover, while previous studies make a short term forecast initialized from the ensemble mean analysis at the last assimilation cycle (Snyder and Zhang 2003; Tong and Xue 2005), this study uses all of the 40 ensemble members at the last assimilation cycle to make an ensemble of forecasts. Two sets of OSSEs are implemented in this study using to assess the benefits of multi parameter ensemble system.

a. Perfect Model Experiment

The ensemble members use the LFO microphysics scheme and the simulated WSR-88D reflectivity and radial velocity observations assimilated are created from the Truth_LFO. Two experiments are conducted using identical background environment. The first experiment (Perfect_Control hereafter) is conducted with the same constant intercept and density parameters for the hydrometeor categories for all ensemble members as in the Truth_LFO. Thus the ensemble members in the Perfect_Control experiment have the identical base environment and microphysics scheme as in the truth but differ from each other in the location and magnitude of the thermal bubbles. The second experiment (Perfect_MP hereafter) also uses the LFO microphysics scheme but instead of using the same constant precipitation particle intercept and density parameters, each ensemble members uses different values for these parameters. Thus the ensemble members in the Perfect_MP experiment differ from each other not only in the location and magnitude of the thermal bubbles but also differ in intercept and density parameters within the same microphysics scheme. These parameters include the intercept parameters for rain (n_{0r}), snow (n_{0s}) and hail/graupel (n_{0h}) and the bulk densities of snow (ρ_s) and hail/graupel (ρ_h). The lists of the different parameter values assigned to the 40 ensemble members in the mulitparameter experiment is shown in Table 2. The use of a variety of density and intercept parameters results in a supercell storms that are different from each other in terms of structure, strength and intensity.

b. Imperfect Model Experiment

Unlike the previous experiment, the synthetic reflectivity and radial velocity observations assimilated by the ensemble members are generated from the Truth_10ICE truth run. The ensemble members in the first experiment (Imperfect_Control hereafter) use the LFO microphysics scheme with the same precipitation particle parameters as in the Perfect_Control experiment. The ensemble members in the second experiment (Imperfect_MP hereafter) also use the LFO microphysics scheme with indentical intercept and density parameters for the precipitation particles as in the Perfect_MP experiment. The initialization and other ensemble configuration details are identical to the previous experiment. The imperfect model experiment explores the performance of the EnKF system for the same storm event in the presence of model errors due to different microphysics scheme used in the ensemble and the truth run.

3. RESULTS

The ultimate goal of storm-scale data assimilation is to obtain accurate short term forecasts of severe storms events. To evaluate the accuracy of the forecasts from assimilating WSR-88D observations for a 30-min period, the 40 analyses from the last assimilation cycles are used as the initial conditions for each of the ensemble members and 1-h short-term forecasts are produced. The accuracy of the analyses and forecasts for both perfect and imperfect model experiments when using fixed or varied microphysics scheme parameters in the ensemble system are then compared with the truth runs. The evaluation criteria include both statistical and graphical comparisons between the truth and the ensemble system. Statistical measures include root-mean-square (rms: Wilks 2006) error of the unobserved variables and equitable threat scores (ETSs: Wilks 2006). The rms error is calculated using the difference between the reference simulation and the ensemble mean analyses and forecasts averaged over only those model grid points where there is convection (the sum of rain, snow and hail mixing ratios are greater than 0.10 g kg^{-1}). The ETS score is calculated from the contingency table that gives discrete joint sample distribution of ensemble mean forecasts and the reference simulation in terms of cell count. An ETS score of 1 denotes a perfect forecast while the forecast accuracy decreases as the ETS scores decreases towards zero.

3.1. Analyses

To evaluate how well the supercell is captured by the ensemble system during the 30- min assimilation period, the rms errors of *u, v* and *w* wind component, temperature and total precipitation (rain, snow and hail/graupel) mixing ratios from the ensemble mean analyses for both perfect and imperfect model experiments are shown in Fig. 2 and Fig. 3 respectively. The rms errors from both experiments are seen to decrease rapidly for all variables as more observations are assimilated. At the end of the assimilation period, the rms errors for winds and temperature variables for the control and multiparameter ensembles from both Perfect (Figs 2a, b, c and d) and Imperfect (Figs 3a, b, c and d) model experiment are very similar. However, while the rms errors of total precipitation mixing ratio from the Perfect_MP experiment are larger than that of the the Perfect_Control experiment (Fig 2e), the rms errors of the same from the Imperfect_MP experiment are significantly smaller than that of the Imperfect_Control experiment (Fig 3e) throughout the 30 minute assimilation period. In the presence of model error, the Imperfect_MP is able to span better the true precipitation mixing ratios and hence produce smaller rms errors.

3.2. *Forecasts*

The rms errors of the ensemble mean forecasts during the 1 hour forecast period for perfect and imperfect model experiment are shown in Fig. 4 and 5 respectively. The quality of the forecast in both plots deteriorates rapidly with time as expected. However, the Perfect_Control experiment yields smaller rms errors compared to the Perfect_MP experiment for the winds, temperature and total precipitation (Fig. 4) variables. In the absence of model error, the EnKF only corrects the errors generated from initial conditions. Moreover, the Perfect_Control experiment uses the same intercept and density parameters as in Truth_LFO, and thus the smaller rms errors are expected. The rms errors for winds and temperature variables (Fig. 5 a, b, c and d) from the Imperfect_MP experiment are very similar to the rms errors from Imperfect_Control experiment during the first 40-mins of the forecast period and yield smaller rms errors during the last 20 min of the forecasts. However, the Imperfect_MP generates smaller rms error than that of the Imperfect_Control for total precipitation mixing ratio (Fig. 5 e) throughout the 1-h forecast period.

To quantify forecast accuracy from the ensemble mean forecasts, ETS scores are calculated by comparing the ensemble mean forecast with the truth for reflectivity values exceeding 35 dBZ threshold and for precipitation (rain, snow and hail/graupel) mixing ratios exceeding 1.0 g/kg threshold. Results indicate that the Imperfect_MP ensemble mean forecasts yield higher ETS scores throughout the 1-h forecast period compared to the that of the Imperfect_Control (Figs.6c and d) for both threshold values. However for the perfect model assumption, the ETS score for the Perfect_Control experiment is larger than the score for the Perfect_MP (Figs.6a and b) for the entire forecast period for both reflectivity and total precipitation mixing ratios.

The total rainfall (mm) at the end of 1-h forecast period accumulated on the ground from the supercell storm is shown in Fig. 7. The accumulated rainfall amounts from the Imperfect_MP ensemble mean forecast (Fig 7c) more closely resembles the truth (Fig. 7a) than the rainfall amounts from the Imperfect_Control (Fig. 7b) experiment. The Imperfect_Control produces higher rainfall amounts from the northern and the southern storms cells when compared to the truth. The maximum mean hail diameter (mm) at the lowest model level during the 1-h forecast period for the perfect and imperfect model experiment is shown in Fig. 8. While the ensemble members from the Perfect_Control (Fig. 8a) do not always capture the truth well within the ensemble members, the truth lies outside the ensemble members for the Imperfect_Control experiment (Fig. 8b). The plot indicates that the ensemble members from the Imperfect_Control experiment overpredict hail diameter. In contrast, the multiparameter experiment from both perfect and imperfect model assumption (Figs. 8 c and d) captures the truth well within the ensemble members.

The ability of the EnKF in forecasting the important variables in convective storm environment is illustrated by comparing the forecast time series of the minimum cold pool temperature, maximum rainwater mixing ratio, maximum hail mixing ratio at the lowest model (100 m) and the maximum vertical vorticity at 300m above ground from each ensemble member for both perfect and imperfect model assumption is shown as in Figs. 9-12. The ensemble members from the control runs for both perfect and the imperfect model experiment provides insufficient ensemble spread, with the truth falling outside the ensemble envelope for different forecast periods. In contrast multiparamter experiments not only improve the ensemble spread, but also capture the truth well within the envelope of the ensemble members.

These results highlight the importance of muliparameter ensemble in the presence of model error. Using a combination of different density and intercept parameters of the hydrometeor category can significantly improve the forecasts over experiments using a single inaccurate intercept and density parameter for the hydrometeor categories. This is especially true when examining the extreme values of the model fields that would be most helpful in determining and identifying potential hazards.

4. DISCUSSION

The goal of this study is to evaluate the feasibility of using a range of intercept and density parameters for the precipitation particle types in the EnKF system in the presence of model error. Two reference simulations of a splitting supercell storm are generated using LFO and 10ICE microphysics schemes in an identical storm environment. Two sets of OSSEs are conducted in an perfect and imperfect model framework using an EnKF data assimilation technique using 1) a constant intercept and density parameters of the hydrometeors for all ensemble members and 2) a range of different values for the intercept and density parameters of the hydrometeors for the different ensemble members. Synthetic WSR-88D reflectivity and radial velocity observations are created from the truth runs using a realistic volume averaging technique and these observations are assimilated into the ensemble system for a 30-min period. The 40 analyses ensemble members from the last assimilation cycle are then used to make 1 h long forecasts.

Results show that the EnKF system performs reasonably well with the imperfect model assumption. It is found that a multiparameter ensemble within the imperfect model framework (Imperfect_MP) generates more accurate forecasts of total precipitation mixing ratios and accumulated rainfall events compared to that of the control imperfect model experiments (Imperfect_Control). This conclusion does not apply for the perfect model assumption where model error does not play a role. Moreover the 1-h forecast time series of the 40 ensemble members for lowest cold pool temperature, maximum hail and rain water mixing ratios at 100 m AGL and the maximum vertical vorticity at 300m AGL indicates that the truth almost always lies within the envelope of ensemble members for the Imperfect_MP experiment while truth more often lies outside the ensemble envelope for the Imperfect_Control experiment. This also holds true for the perfect model assumptions. Moreover the multiparameter experiments also yields a better ensemble spread.

Caution is warranted as the results obtained in these studies are based on synthetic radar observations. Moreover, in a real observation assimilation, the model error can potentially be larger than that considered in this study. The possibility of using multiparameter ensemble in storm-scale data assimilation system should be tested using a broader range of experiments using real radar observations of severe weather events. However, these results suggest that the inclusion of a range of intercept and density parameters in a convection resolving ensemble system can provide improved short range forecasts for a wide range of storm systems.

Acknowledgments. The authors are indebted to Ted Mansell for his valuable suggestions. The authors also are grateful to David Dowell and Louis Wicker for help with the COMMAS model. Local computer assistance provided by Brett Morrow, Steven Fletcher, Brad Swagowitz, and Karen Cooper are greatly appreciated. Partial funding for this research was provided by NOAA/Office of Oceanic and Atmospheric Research under NOAA-University of Oklahoma Cooperative Agreement #NA17RJ1227, U.S. Department of Commerce.

REFERENCES

Aksoy, A., D. Dowell, and C. Snyder, 2009: Ensemble Kalman filter assimilation of real radar observations: A multi-case comparative study of storm-scale forecasts and analyses. *Mon. Wea. Rev.*, **137**, 1805-1824. DOI: 10.1175/2008MWR2691.1

Brandes, E. A., K. Ikeda, G. Zhang, M. Schönhuber, and R. M. Rasmussen, 2007: A statistical and physical description of hydrometeor distributions in Colorado snowstorms using a video disdrometer. *J. Appl. Meteor. Climatol.,* **46,** 634–650.

Cifelli, R., C. R. Williams, D. K. Rajopadhyaya, S. K. Avery, K. S. Gage, and P. T. May, 2000: Drop-size distribution characteristics in tropical mesoscale convective systems. *J. Appl. Meteor.,* **39,** 760–777.

Coniglio, M.C., D.J. Stensrud, and L.J. Wicker, 2006: Effects of upper-level shear on the structure and maintenance of strong quasi-linear mesoscale convective systems. *J. Atmos. Sci.*, **63**, 1231-1252.

Dowell, D. C. , and L. J. Wicker, 2008: Additive noise for storm-scale ensemble forecasting and data assimilation. Submitted to *J. Atmos. Oceanic Technol*.

________, F. Zhang, L. J. Wicker, C. Snyder, and N.A. Crook, 2004a: Wind and temperature retrievals in the 17 May 1981 Arcadia, Oklahoma, supercell: Ensemble Kalman filter experiments. *Mon. Wea. Rev.*, **132**, 1982-2005.

________, L. J. Wicker, and D. J. Stensrud, 2004b: High resolution analyses of the 8 May 2003 Oklahoma City storm. Part II: EnKF data assimilation and forecast experiments. Preprints, *22nd Conf. Severe Local Storms*, Hyannis, MA, Amer. Meteor. Soc.

Fujita, T., Stensrud D. J., Dowell D. C., 2007: Surface data assimilation using an ensemble Kalman filter approach with initial condition and model physics uncertainty. *Mon. Wea. Rev.,* **135,** 1846-1868.

Gilmore, M.S., J.M. Straka, and E.N. Rasmussen, 2004: Precipitation uncertainty due to variations in precipitation particle parameters within a simple microphysics scheme. *Mon. Wea. Rev*., 2004, **132**, 2610-2627.

Gunn, K. L. S., and J. S. Marshall, 1958: The distribution with size of aggregate snowflakes. *J. Meteor.,* **15,** 452–461.

Houze, R. A., Jr., P. V. Hobbs, P. H. Herzegh, and D. B. Parsons, 1979: Size distributions of precipitation particles in frontal clouds. *J. Atmos. Sci.,* **36,** 156–162.

——, C.-P. Cheng, C. A. Leary, and J. F. Gamache, 1980: Diagnosis of cloud mass and heat fluxes from radar and synoptic data. *J. Atmos. Sci.,* **37,** 754–773.

Lin, Y.-L., R.D. Farley, and H.D. Orville, 1983: Bulk parameterization of the snow field in a cloud model. *J. Appl. Meteor*., **22**, 1065-1092.

Lord, S. J., E. Kalnay, R. Daley, G. D. Emmitt, and R. Atlas, 1997: Using OSSEs in the design of the future generation of integrated observing systems. Preprints, *First Symp. on Integrated Observation Systems*, Long Beach, CA, Amer. Meteor. Soc., 45–47.

Marshall, J.S., and McK. Palmer, 1948: The distribution of raindrops with size. *J. Atmos. Sci*., **5**, 165-166.

Mitchell, D. L., 1988: Evolution of snow-size spectra in cyclonic storms. Part I: Snow growth by vapor deposition and aggregation. *J. Atmos. Sci.,* **45,** 3431–3451.

Pruppacher, H. R., and J. D. Klett, 1978: *Microphysics of Clouds and Precipitation*. Reidel, 714 pp.

Stensrud, D. J. 2007: *Parameterization Schemes: Keys to Understanding Numerical Weather Prediction Models.* Cambridge University Press, 459 pp.

________, N. Yussouf, D. C. Dowell and M. C. Coniglio, 2009: Assimilating surface data into a mesoscale model ensemble: Cold pool analyses from spring 2007. *Atmos. Res,* **93,** 207-220

Snook, N. and M. Xue, 2008: Effects of microphysical drop size distribution on tornadogenesis in supercell thunderstorms. *Geophy. Res. Letters,* **35**, L24803, doi:10.1029/2008GL035866

Snyder, C. and F. Zhang, 2003: Assimilation of simulated Doppler radar observations with an ensemble Kalman filter. *Mon. Wea. Rev.*, **131**, 1663-1677.

Straka, J.M., and E.R. Mansell, 2005: A Bulk Microphysics Parameterization with Multiple Ice Precipitation Categories. *J. Appl. Meteor.*, **44**, 445–466.

Tong, M. and M. Xue, 2005: Ensemble Kalman filter assimilation of Doppler radar data with a compressible nonhydrostatic model: OSS experiments. *Mon. Wea. Rev.*, **133**, 1789-1807.

van den Heever, S. C., and W. R. Cotton, 2004: The impact of hail size on simulated supercell storms. *J. Atmos. Sci.,* **61,** 1596–1609.

Weisman, M. L. and J. B. Klemp, 1982: The dependence of numerically simulated convective storms on vertical wind shear and buoyancy. *Mon. Wea. Rev.*, **110**, 504-520.

Whitaker, J. S., and T. M. Hamill, 2002: Ensemble data assimilation without perturbed observations. *Mon. Wea. Rev.*, **130**, 1913-1924.

Wicker, L. J., and W. C. Skamarock, 2002: Time-splitting methods for elastic models using forward time schemes. *Mon. Wea. Rev.*, **130**, 2088-2097.

Wilks, D. S., 2006: *Statistical Methods in the Atmospheric Sciences: Second Edition.* Academic Press, Boston, MA, 627 pp.

Wood, V. T., R. A. Brown, and D. Dowell, 2009: Simulated WSR-88D Velocity and Reflectivity Signatures of Numerically-Modeled Tornadoes. *J. Atmos. Oceanic Technol.* 26(5): 876.

Xue, M., M. Tong, and K.K. Droegemeier, 2006: An OSSE framework based on the ensemble square root Kalman filter for evaluating the impact of data from radar networks on thunderstorm analysis and forecasting. *J. Atmos. Oceanic Technol*., 23, 46-66.

Zhang, F., C. Snyder, and J. Sun, 2004: Impacts of initial estimate and observation availability on convective-scale data assimilation with an ensemble Kalman filter. *Mon. Wea. Rev.*, **132**, 1238-1253.

Table 1. The intercept and the density parameters for the precipitation particles from the Truth_LFO and Truth_10ICE simulations.

LFO Scheme			10 ICE Scheme		
Catagory	Intercept m^{-4}	Density kg m^{-3}	Catagory	Intercept m^{-4}	Density kg m^{-3}
Hail/Graupel	$4x10^4$	900	Graupel (low)	$4.0x10^5$	300
Snow	$3x10^6$	100	Graupel (medium)	$2.0x10^5$	500
Rain	$8x10^6$	1000	Graupel (high)	$1.0x10^5$	700
Ice	-	-	Frozen drops	$4.0x10^5$	800
			Small hail	$4.0x10^4$	800
			Large hail	$1.0x10^3$	900
			Snow	$8x10^6$	100
			Rain	$8x10^6$	1000
			Rimed ice	$1.0x10^8$	300
			Plate ice	-	900
			Column ice	-	900
			Cloud droplets	-	1000

Table 2. List of ensemble members with the values of intercept parameters and densities of rain, hail/graupel and snow particles from the LFO microphysics scheme.

Ensemble Members	Hail/graupel intercept n_{0h} (m^{-4})	Density of hail/graupel ρ_h (kg m^{-3})	Snow intercept n_{0s} (m^{-4})	Density of snow ρ_s (kg m^{-3})	Rain intercept n_{0r} (m^{-4})
1	4.00×10^4	900	3.00×10^6	100	8.00×10^6
2	4.50×10^3	900	1.04×10^7	50	7.14×10^6
3	5.07×10^3	800	6.77×10^6	100	5.19×10^6
4	5.70×10^3	500	2.18×10^6	350	1.22×10^7
5	6.41×10^3	700	1.89×10^6	400	6.09×10^6
6	7.22×10^3	600	8.38×10^6	250	9.32×10^6
7	8.12×10^3	800	7.27×10^6	150	2.70×10^7
8	9.14×10^3	900	3.84×10^6	50	2.30×10^7
9	1.03×10^4	400	1.76×10^6	200	4.43×10^6
10	1.16×10^4	500	1.43×10^6	300	1.09×10^7
11	1.30×10^4	600	1.07×10^6	400	8.38×10^6
12	1.47×10^4	700	2.89×10^6	250	7.53×10^6
13	1.65×10^4	800	5.10×10^6	150	5.77×10^6
14	1.86×10^4	900	8.99×10^6	300	3.16×10^7
15	2.09×10^4	400	1.38×10^7	100	8.83×10^6
16	2.35×10^4	500	2.51×10^6	300	4.20×10^6
17	2.65×10^4	600	2.34×10^6	100	3.00×10^7
18	2.98×10^4	700	1.53×10^6	150	1.96×10^7
19	3.35×10^4	800	7.80×10^6	200	1.76×10^7
20	3.77×10^4	900	1.33×10^6	100	1.58×10^7
21	4.24×10^4	400	4.12×10^6	350	2.18×10^7
22	4.78×10^4	500	4.43×10^6	100	1.50×10^7
23	5.37×10^4	600	5.48×10^6	250	2.56×10^7
24	6.05×10^4	700	3.58×10^6	400	1.35×10^7
25	6.80×10^4	800	1.00×10^6	20	6.42×10^6
26	7.66×10^4	400	1.28×10^7	300	3.98×10^6
27	8.62×10^4	500	5.88×10^6	200	2.42×10^7
28	9.70×10^4	900	1.15×10^6	50	1.28×10^7
29	1.09×10^5	400	1.24×10^6	350	4.67×10^6
30	1.23×10^5	700	2.03×10^6	50	2.07×10^7
31	1.38×10^5	800	9.65×10^6	350	1.04×10^7
32	1.56×10^5	900	1.19×10^7	200	5.48×10^6
33	1.75×10^5	500	1.64×10^6	250	9.82×10^6
34	1.97×10^5	600	6.31×10^6	400	1.67×10^7
35	2.22×10^5	700	1.11×10^7	100	1.15×10^7
36	2.49×10^5	800	4.75×10^6	300	2.84×10^7
37	2.81×10^5	900	2.70×10^6	150	1.86×10^7
38	3.16×10^5	400	1.48×10^7	50	7.94×10^6
39	3.55×10^5	700	1.58×10^7	400	4.92×10^6
40	4.00×10^5	900	3.33×10^6	300	6.77×10^6

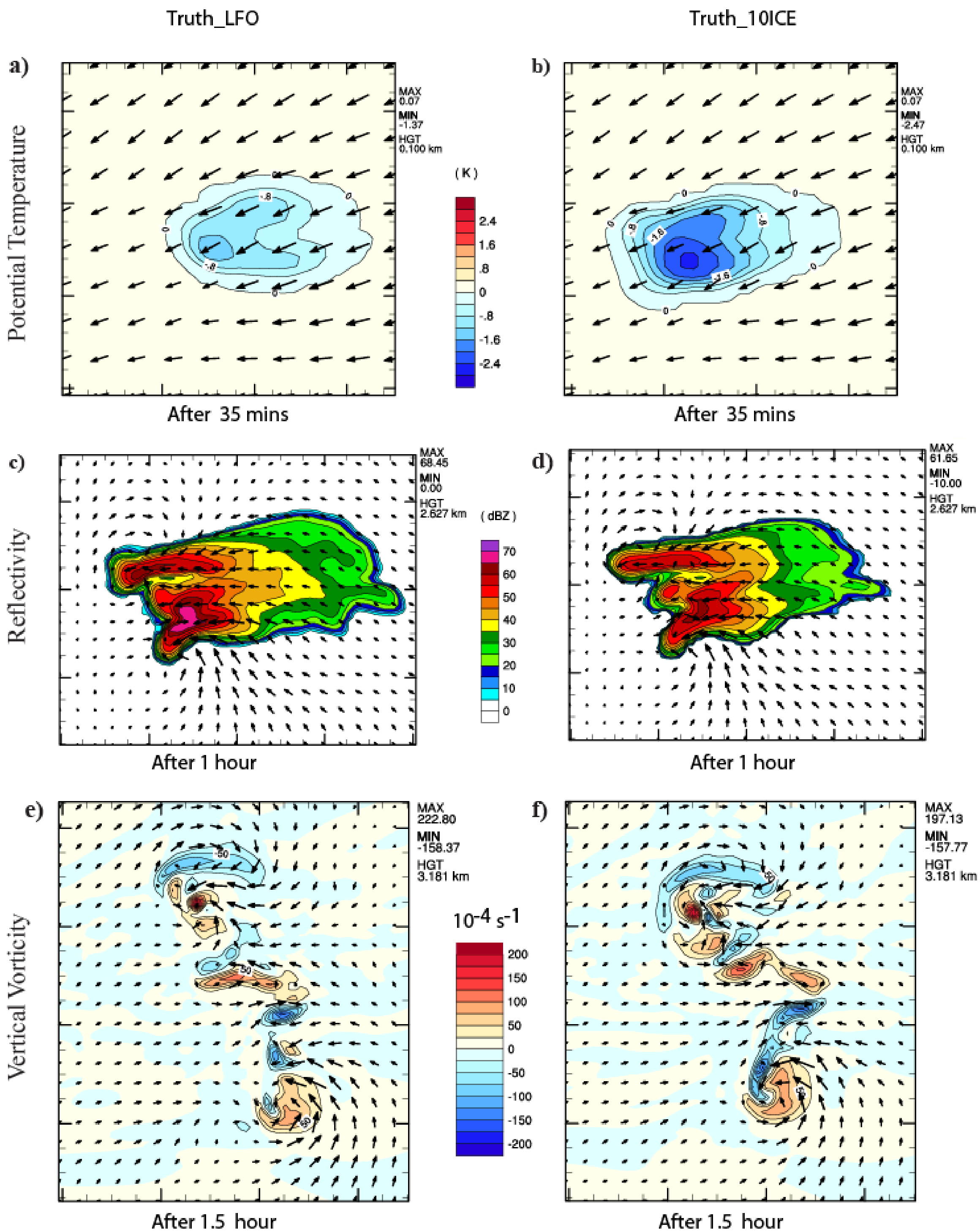

Figure 1. Potential temperature after 35 minutes of the simulation at the lowest model level (100 m AGL) (a and b), reflectivity (c and d) 2.6 km AGL after 1 hr and vertical vorticity (e and f) at 3.1 km AGL after 1.5 hr from the truth simulation using the LFO and 10 ICE microphysics scheme.

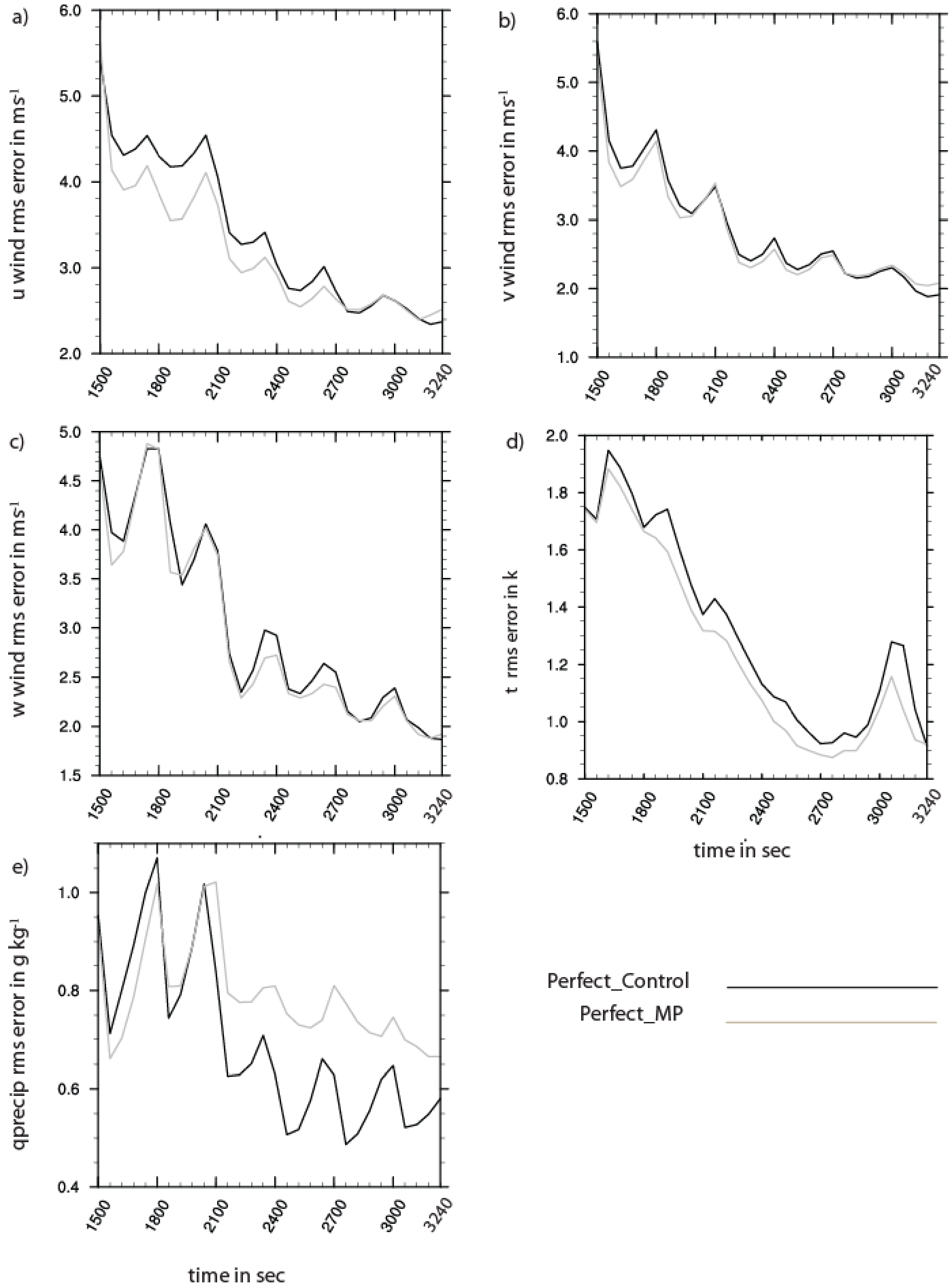

Figure 2. The rms errors of ensemble mean analyses vs. time(sec) during the 30-min assimilation periiod from the perfect model experiment starting at t = 25 min and ending at t = 54 min for (a) u (m s^{-1}), (b) v (m s^{-1}), (c) w (m s^{-1}), (d) t (k) and (e) total precipitation (rain, snow, hail/graupel) mixing ratios (g kg^{-1}) for the control (black lines) and muliparameter (gray lines) ensemble system. Values are averaged over the domain at grid points where the total precipitation mixing ratios (sum of qr, qh and qs) in the truth run is greater than 0.10g kg^{-1}.

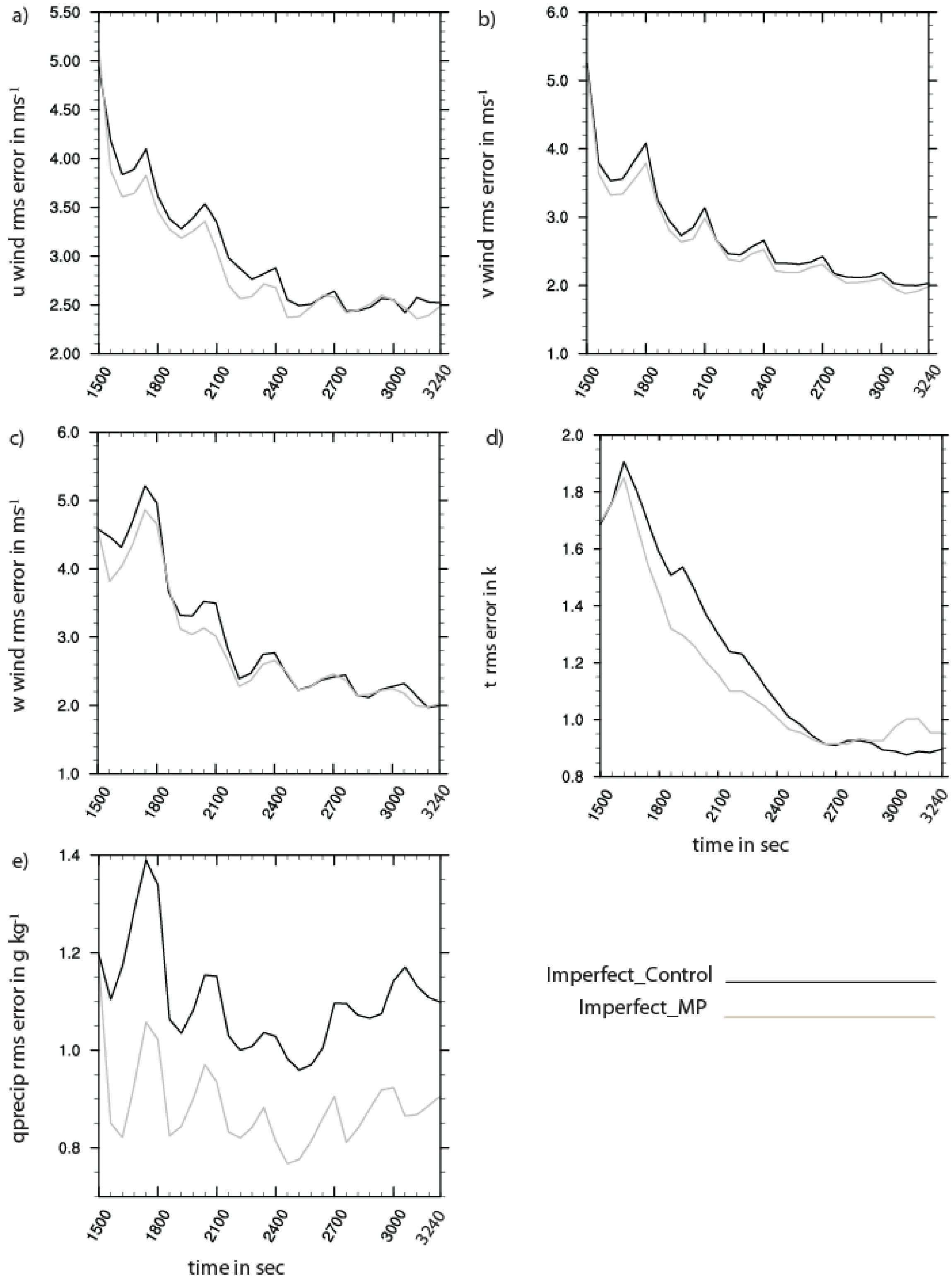

Figure 3. Same as in Fig. 2 but for the imperfect model experiment.

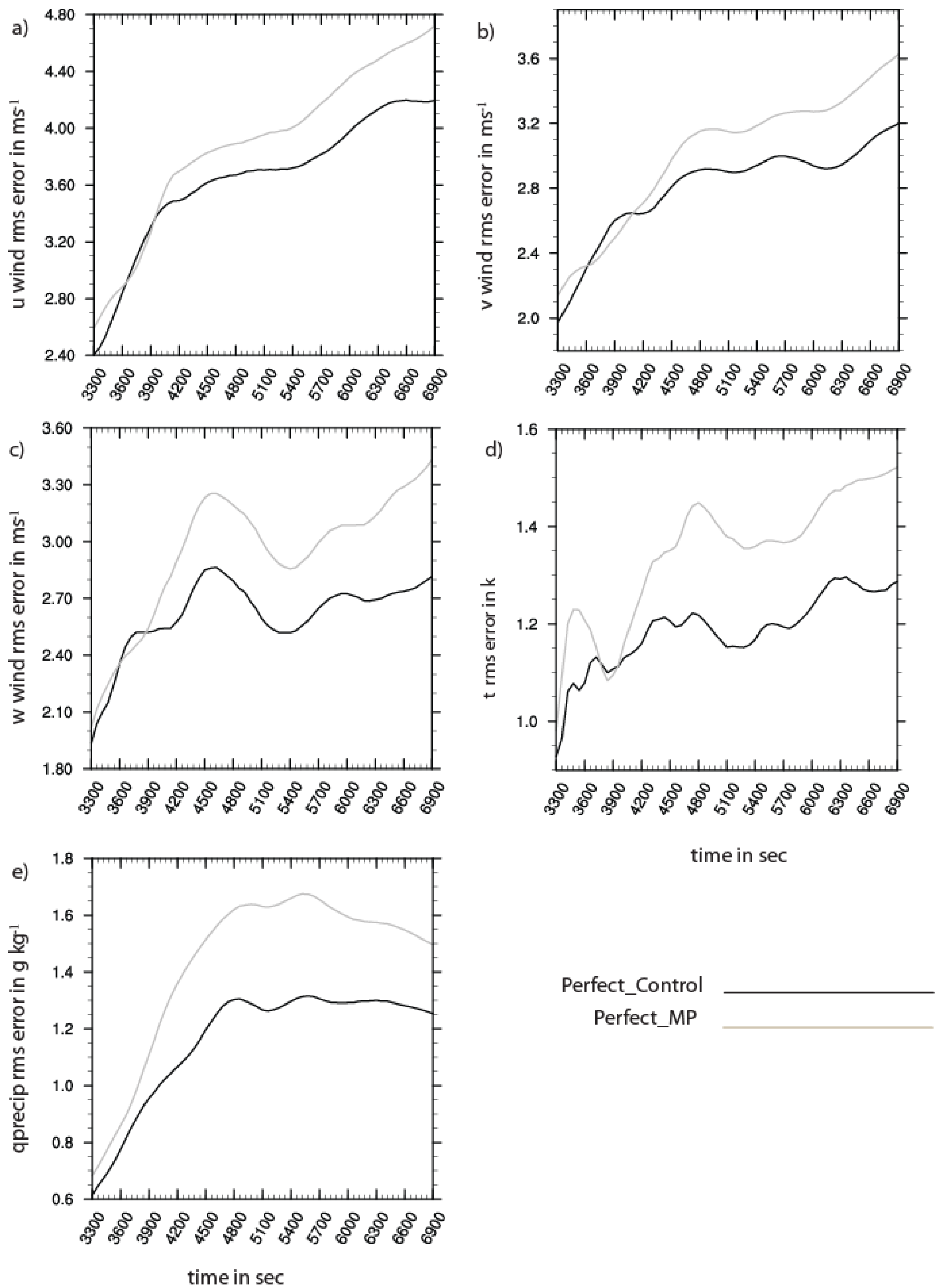

Figure 4. The rms errors of ensemble mean forecast during the 1 hr forecast period for (a) u (m s^{-1}), (b) v (m s^{-1}), (c) w (m s^{-1}), (d) t (k) and (e) total precipitation (rain, snow, hail/graupel) mixing ratios (g kg^{-1}). Values are averaged over the domain where the total precipitation (sum of qr, qh and qs mixing ratios) is greater than 0.10g kg^{-1}. Details are shown in the legend.

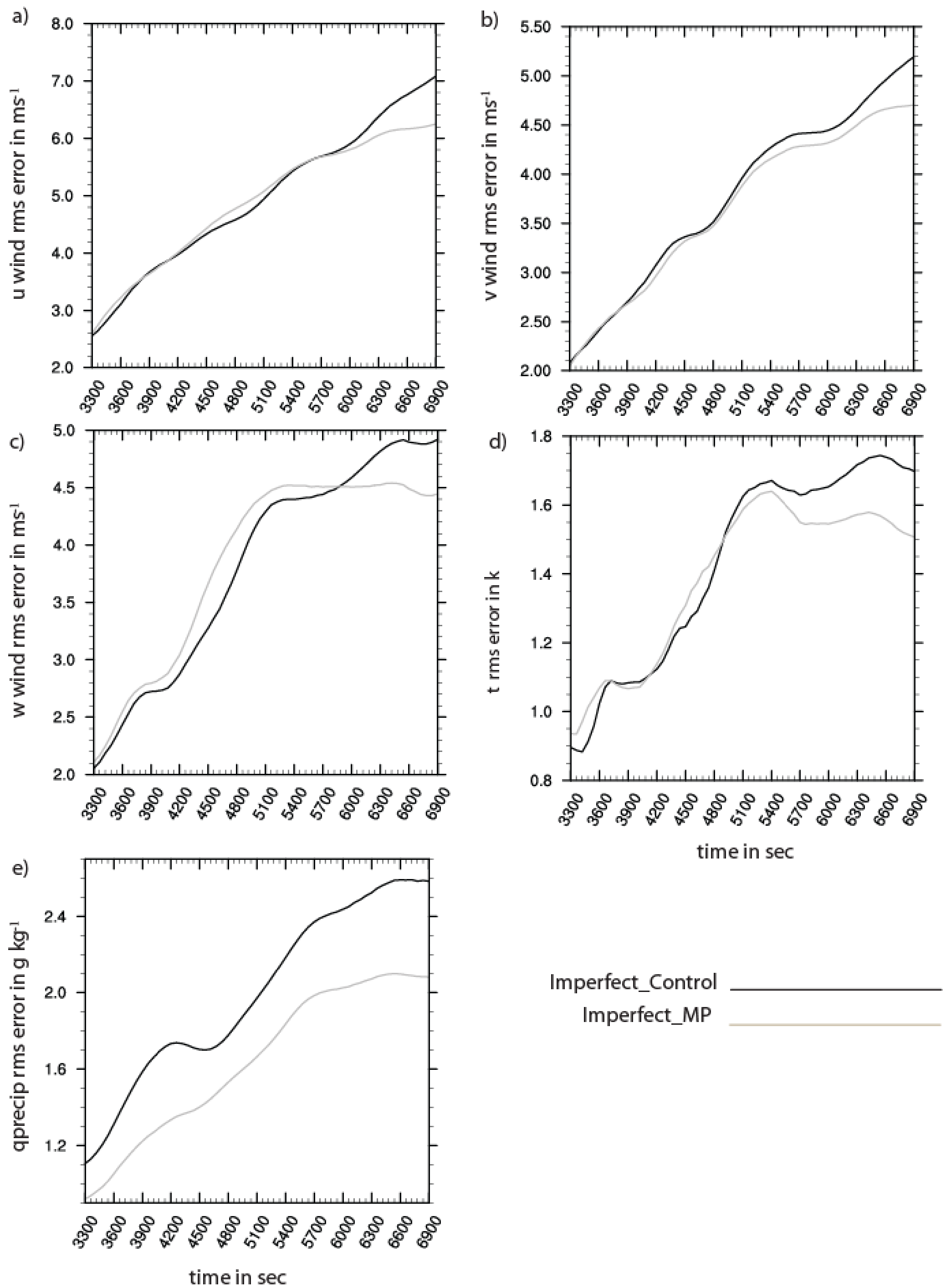

Figure 5. Same as in Fig. 4 but for the imperfect model experiment.

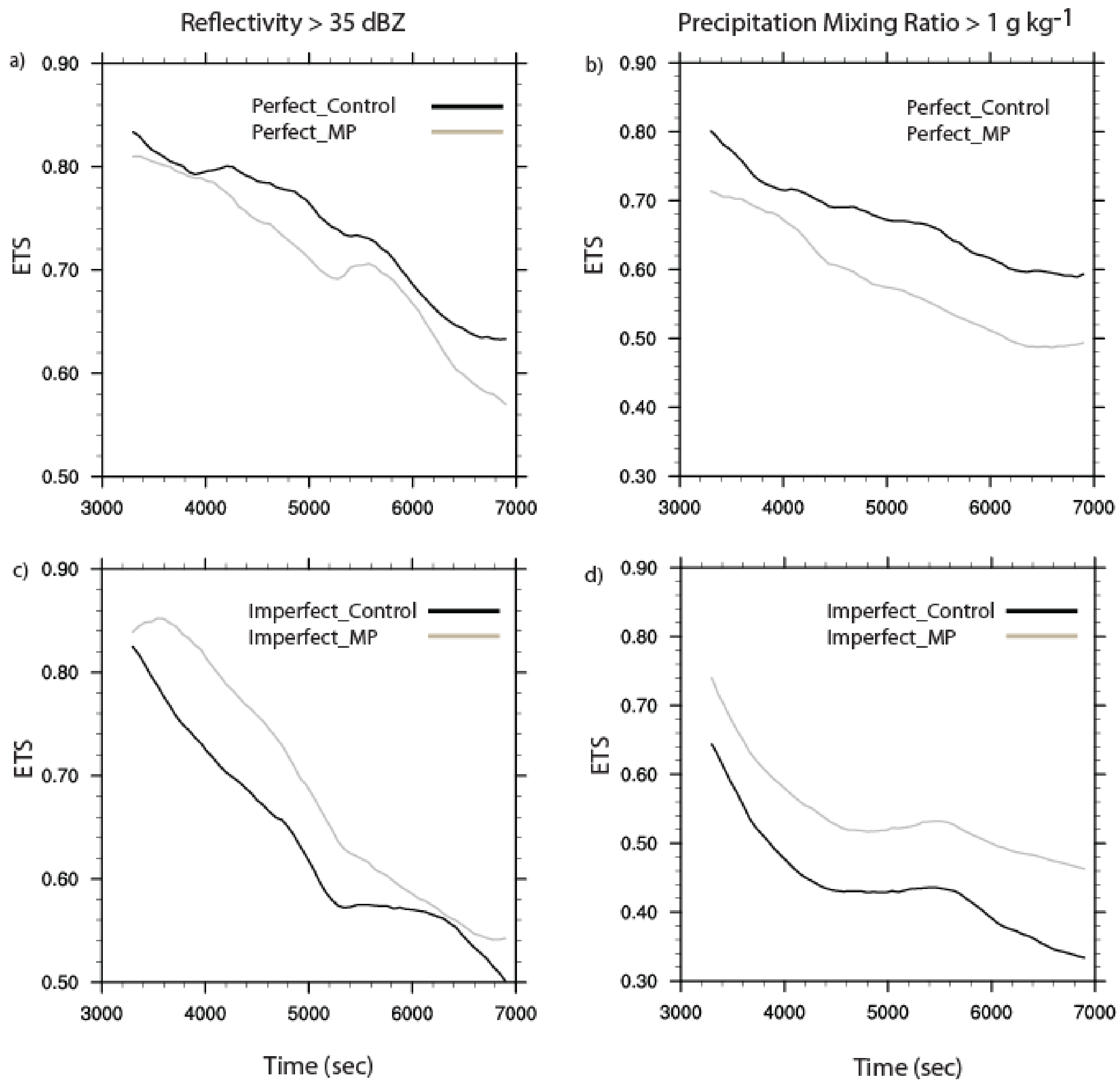

Figure 6. Values of equitable threat score (ETS) for reflectivity values exceeding 35 dBZ threshold for a) Perfect and c) Imperfect Model experiments and the precipitation (rain, snow and hail/graupel) mixing ratios exceeding 1.0 g/kg threshold for c) Perfect and d) Imperfect Model experiments as function of forecast time (sec). Details are shown in legends

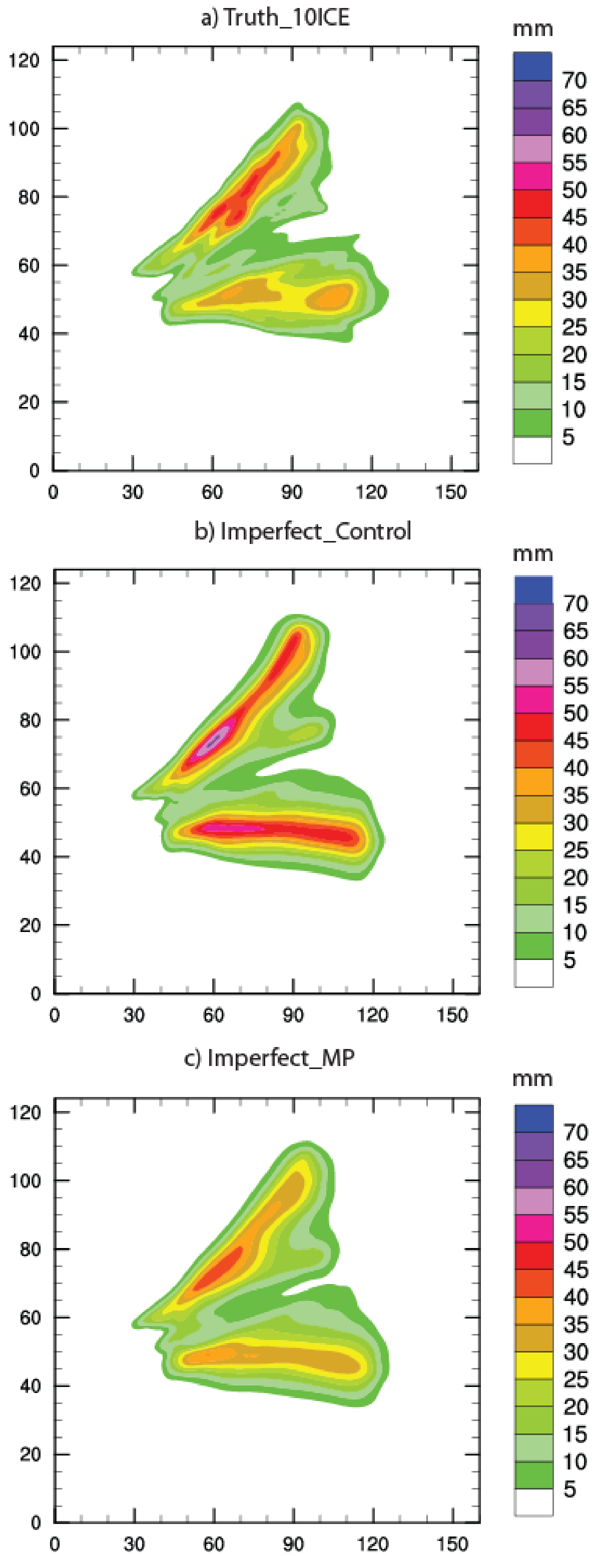

Figure 7. 1-h accumulated rainfall (mm) amounts from the a) Truth_10ICE and the ensemble mean forecasts of 1-h accumulated rainfall (mm) from b) Imperfect_Control and c) Imperfect_MP experiment.

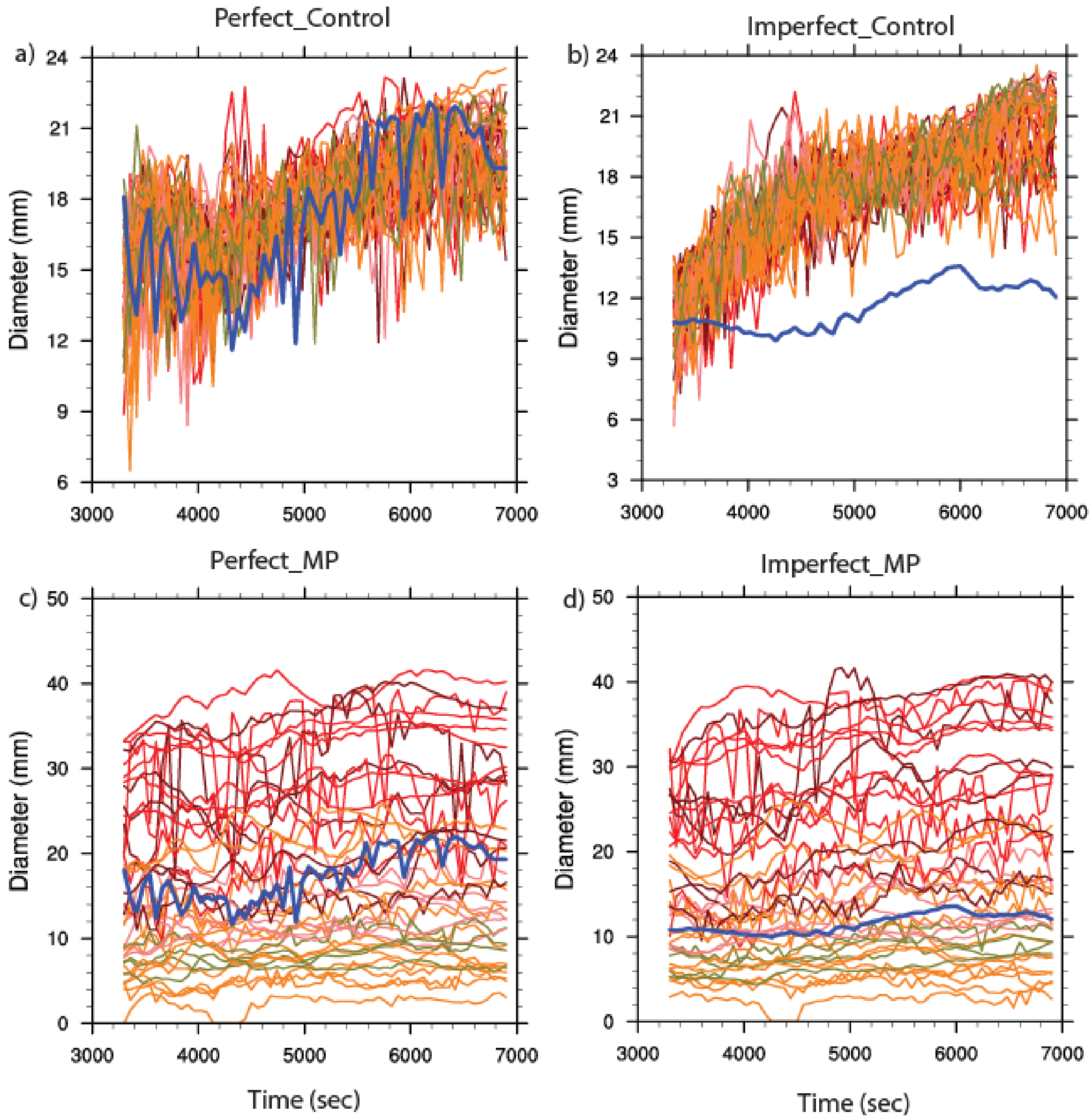

Figure 8. The maximum mean hail diameter (mm) at the lowest model level (100m AGL) during the 1-h forecast period for a) Perfect_Control, b) Imperfect_Control c) Perfect_MP, and d) Imperfect_MP experiment.

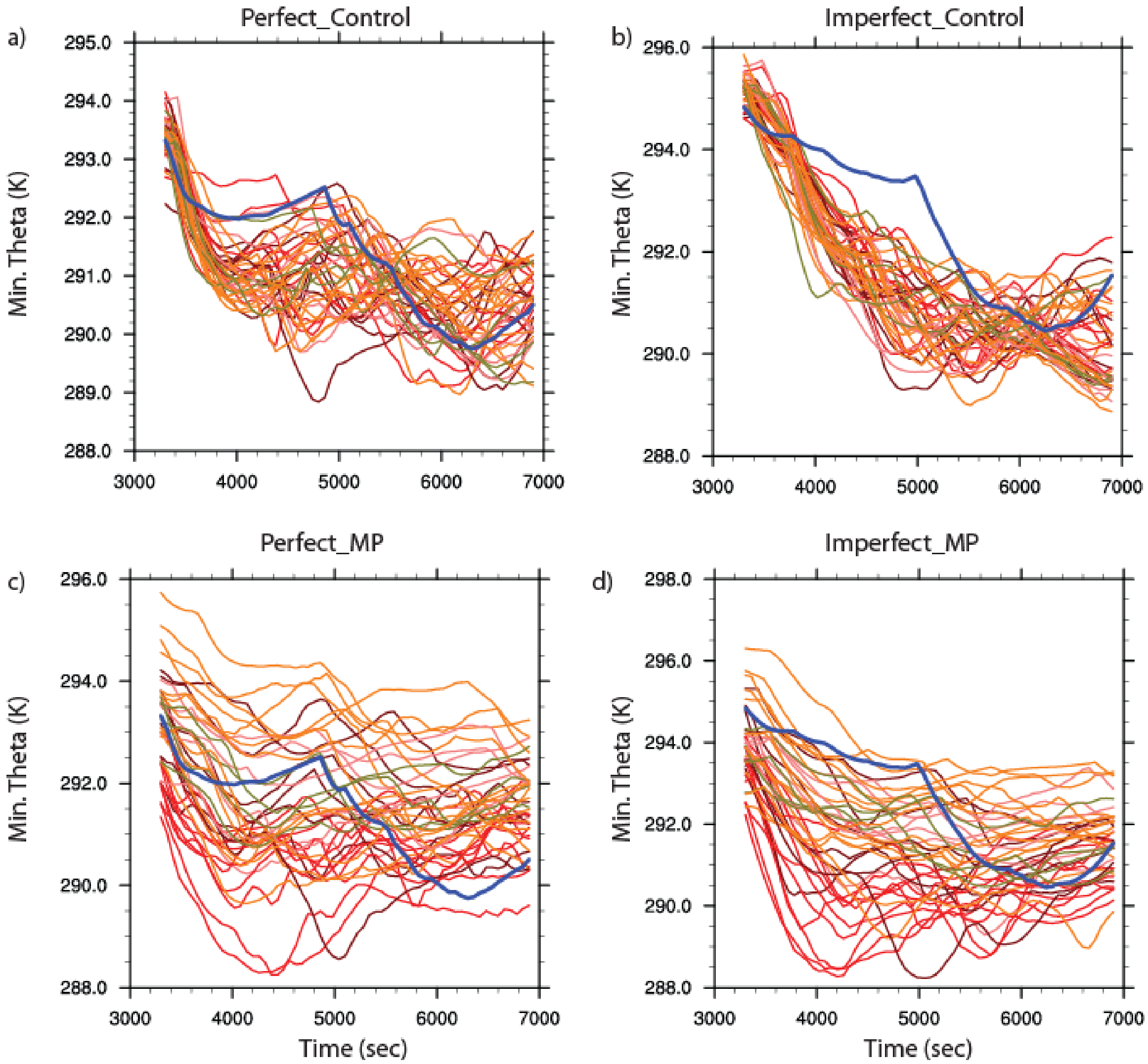

Figure 9. The minimum potential temperature (k) at the lowest model level (100m) during the 1-h forecast period for all the 40 ensemble members (in different shades of red) and the truth (in blue) for a) Perfect_Control, b) Imperfect_Control, c) Perfect_MP and d) Imperfect_MP experiment.

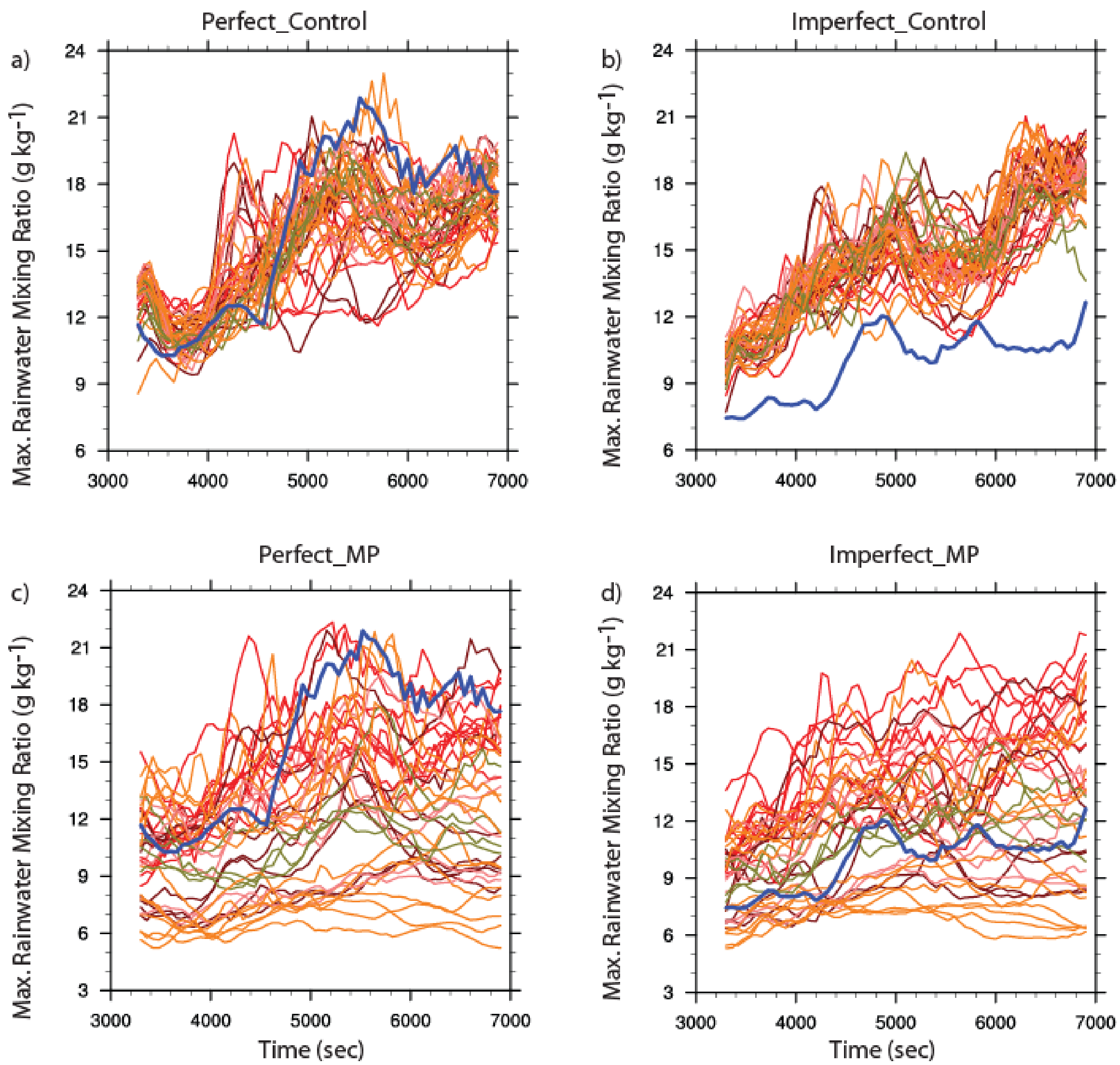

Figure 10. Same as in Fig. 9 but for maximum rainwater mixing ratio (g kg^{-1}).

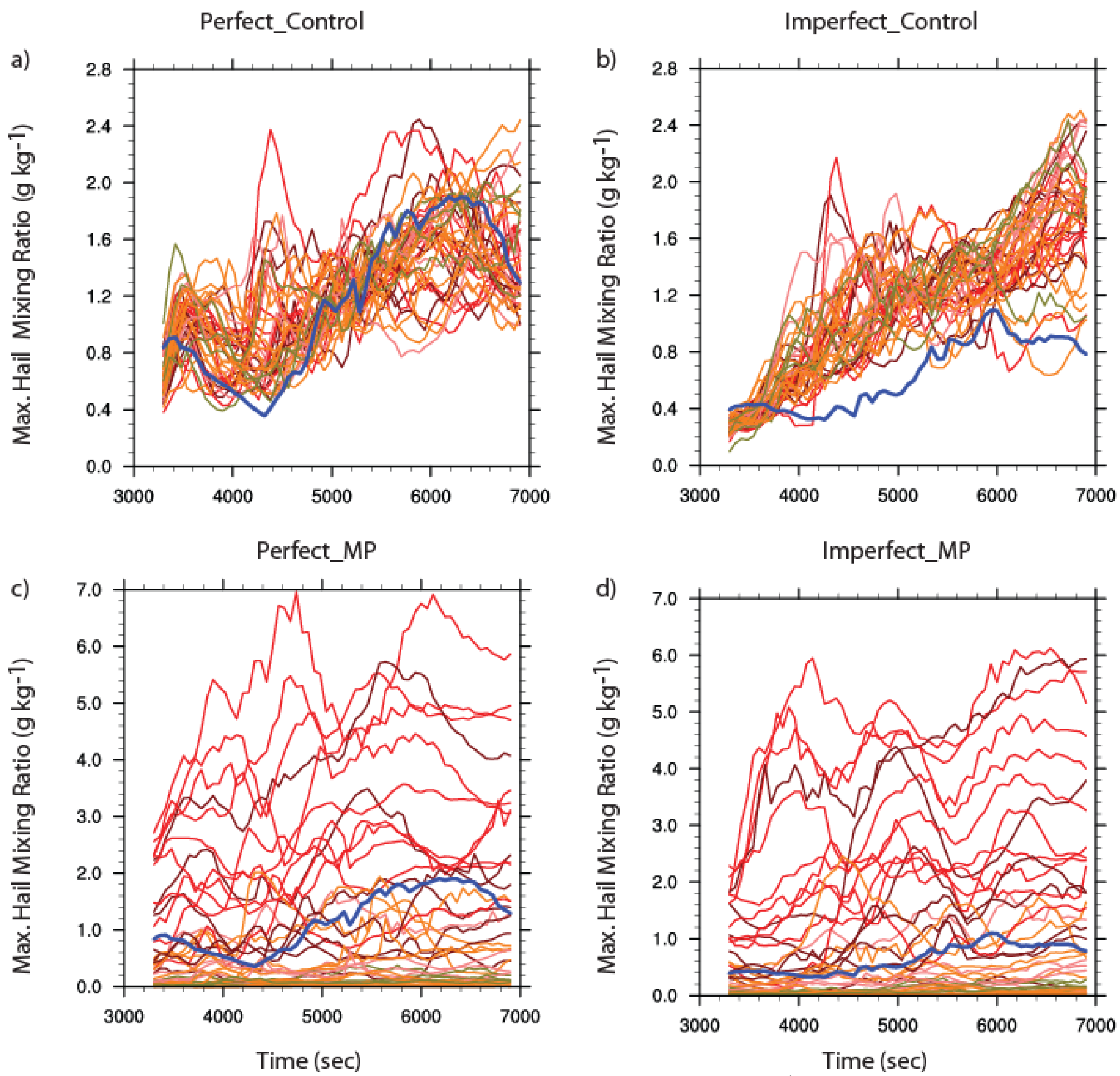

Figure 11. Same as in Fig. 9 but for maximum hail mixing ratio (g kg^{-1}).

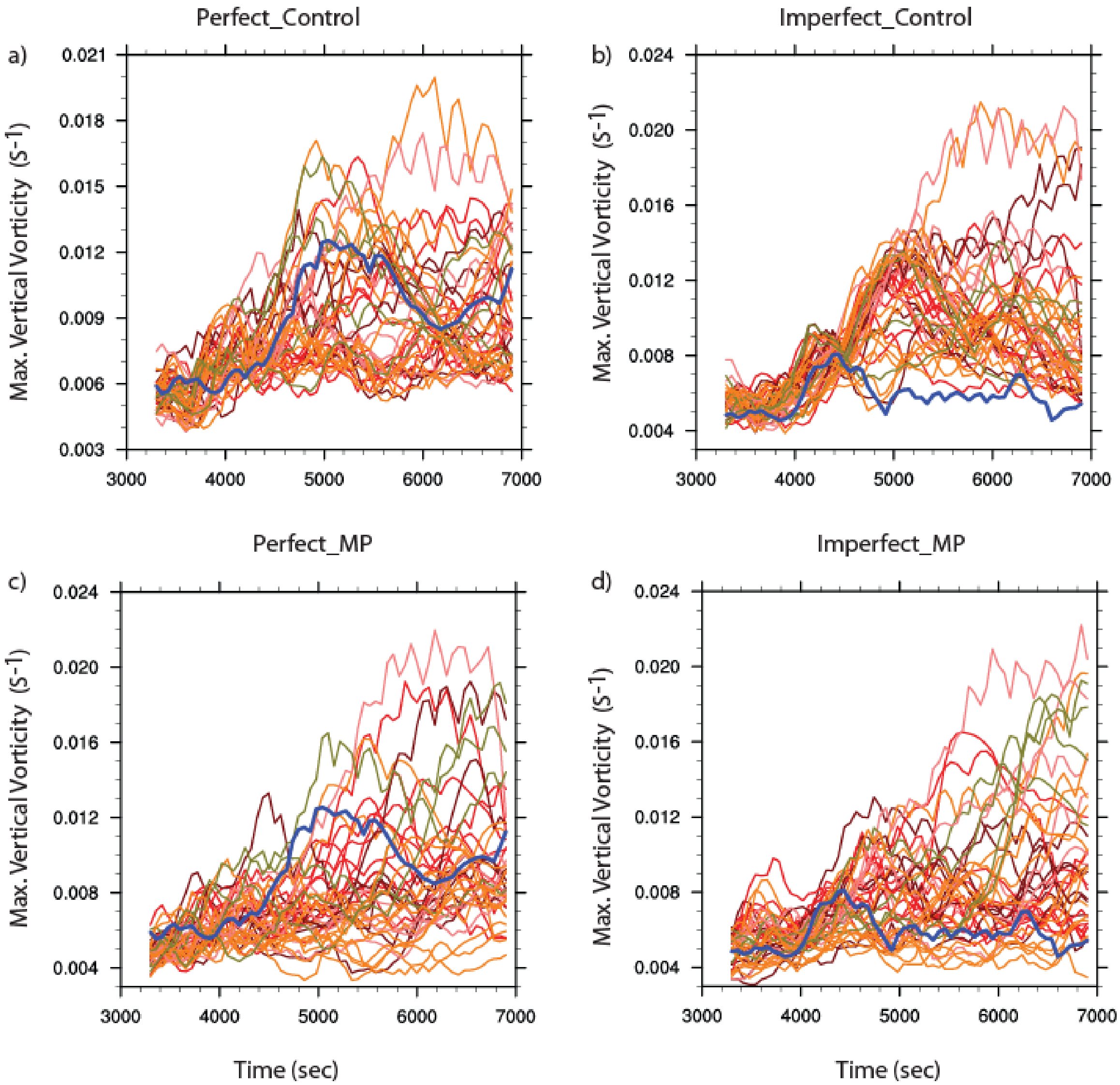

Figure 12. Same as in Fig. 9 but for maximum vertical vorticity (s^{-1}) at 300m AGL.